Desalination and Water Treatment
www.deswater.com
doi: 10.5004/dwt.2023.29924

308 (2023) 229–243
October

Elevating pH and introducing SO_4^{2-} to promote organic dye mineralization by UV/PDS process under high contents of Cl^- conditions

Bing Yang[a,b,c,*], Xiangfu Huang[b], Yucheng Liu[b,c,*], Mi Zhou[b], Wei Jiang[d], Qinman Li[b], Qiuping Luo[b], Lili Ma[b], Lingli Li[b]

[a]*Oil & Gas Field Applied Chemistry Key Laboratory of Sichuan Province, Southwest Petroleum University, Chengdu, Sichuan 610500, China, email: yangb2016@swpu.edu.cn (B. Yang)*
[b]*College of Chemistry and Chemical Engineering, Southwest Petroleum University, Chengdu, Sichuan 610500, China, emails: rehuo2013@sina.cn (Y. Liu), 2742389864@qq.com (X. Huang), 709772834@qq.com (M. Zhou), 327662625@qq.com (Q. Li), 3400932086@qq.com (Q. Luo), hjxymall@163.com (L. Ma), lingli@swpu.edu.cn (L. Li)*
[c]*Institute of Industrial Hazardous Waste Disposal and Utilization, Southwest Petroleum University, Chengdu, Sichuan 610500, China*
[d]*Chengdu Central Radiation Environmental Monitoring and Control Technologies, Ltd., Chengdu, Sichuan 610500, China, email: 4287705@qq.com (W. Jiang)*

Received 23 June 2023; Accepted 27 August 2023

ABSTRACT

The removal of organic pollutants by sulfate radical ($SO_4^{\bullet-}$)-based advanced oxidation processes (SR-AOPs) would be seriously inhibited in the presence of chloride ions (Cl^-). In this study, the effects of different conditions of pH and SO_4^{2-} on Orange II (OrgII) decolorization and mineralization treated by ultraviolet/sodium persulfate (UV/PDS) in the presence of Cl^- were investigated. OrgII mineralization was significantly inhibited (70%) in the presence of Cl^-, which was attributed to that the produced chlorine radicals ($Cl^\bullet$ and $Cl_2^{\bullet-}$) and free chlorine (Cl_2 and HClO) could not decompose OrgII completely and, more importantly, the chlorinated intermediate products would compete with PDS to absorb ultraviolet light. Elevating pH from 3 to 10 greatly enhanced total organic carbon (TOC) removal rates by 46% and 16%, respectively, with Cl^- at 200 and 1,000 mM, which was attributed to that more $^\bullet OH$ generated under pH 10 would decrease the generation of chlorinated byproducts and promote the mineralization process. Adding SO_4^{2-} at 50 and 100 mM improved OrgII mineralization (3%–10%) with Cl^- at 100 mM due to the reaction between SO_4^{2-} and $Cl^\bullet$ to regenerate $SO_4^{\bullet-}$ and the reduction of the chlorination products to improve the ultraviolet light absorption of PDS. However, SO_4^{2-} at high concentration (200 and 500 mM) may cause the reduction of $SO_4^{\bullet-}$ redox potential to decrease TOC removal (8%–26%). This study reveals the complex influencing mechanism of Cl^- contents under different pH and SO_4^{2-} conditions on the removal of organic pollutants by UV/PDS and suggests the possible regulating methods for the application of SR-AOPs to the pretreatment of high salinity organic wastewater.

Keywords: Orange II; Sulfate radical; Chloride ion; High salinity organic wastewater; Advanced oxidation processes (AOPs)

1. Introduction

High salinity organic wastewater (HSOW) widely comes from oil and gas field exploitation, petrochemical industry, landfill leachate, textile, paper, and flue gas desulfurization. Inorganic anions (e.g., chloride, Cl^-; sulfate, SO_4^{2-}) are common in HSOW: flowback water contains up to 270,000 mg/L·Cl^- and 763 mg/L·SO_4^{2-}, and desulfurization wastewater

* Corresponding authors.

contains up to 17,204 mg/L·Cl^- and 6,453 mg/L·SO_4^{2-} [1–5]. At present, the wide application of membrane technology provides a reliable treatment for reclaiming water from different wastewater streams for re-use and obtaining industrial grade salt [6]. Therefore, pretreatments for organics removal in HSOW are needed to reduce membrane contamination and extend the service life of membrane system [7]. However, the poor biodegradability of HSOW due to the high salt content and complex composition limits the application of biochemical treatment [8]. Although high content of Cl^- in HSOW may pose a certain inhibition on the removal of organic compounds by advanced oxidation processes (AOPs) [9–13], hydroxyl radical (•OH)-based AOPs (HR-AOPs) such as Fenton oxidation [14], catalytic ozone oxidation [15], and UV/H_2O_2 [16] have been widely applied for HSOW pretreatment to remove organics due to the resistance of HR-AOPs to Cl^- inhibition [17,18].

The sulfate radical ($SO_4^{\bullet-}$)-based on advanced oxidation processes (SR-AOPs) has been extensively explored for the oxidative removal of many organic pollutants [11,19–21] due to the high potential of $SO_4^{\bullet-}$ (E^0 = 2.5–3.1 V) [22] and applicability over a wide pH range [23]. $SO_4^{\bullet-}$ produced in SR-AOPs [Eq. (1)] (Table 1) is more selective than •OH produced in HR-AOPs to react with certain organics [24], such as trichloroethylene [25], enoxacin [26], antibiotic florfenicol [27], and ibuprofen [28]. However, Cl^- at high content may greatly impact the mineralization of organic matter in HSOW treated by SR-AOPs via quickly scavenging $SO_4^{\bullet-}$ to produce $Cl^\bullet$ ($k = 2.7 \times 10^8$ M/s) [Eq. (3)] and then $Cl_2^{\bullet-}$ ($k = 8.5 \times 10^9$ M/s) [Eq. (5)] [29,30]. The varied reactivities of chlorine radicals ($Cl^\bullet$ and $Cl_2^{\bullet-}$) towards different organics with reaction rate constants ranging from 10^6 to 10^{10} M/s [31–33] would pose various influences on the removal of organic pollutants by SR-AOPs. Previous studies have shown that Cl^- inhibited the degradation of sulfa chloropyrazine [34], carbon tetrachloride [35], and ketoprofen [36] by thermally activated sodium persulfate (PDS). Moreover, the effect of Cl^- at low content on the degradation of azo dyes shows a dual effect of first inhibition and then promotion. The degradation of azo dyes is inhibited under low content of Cl^- (<10 mM) related to the increase of chlorine radicals ($Cl^\bullet$, $Cl_2^{\bullet-}$) with relatively low redox potential and the reduction of $SO_4^{\bullet-}$. The dominant reaction is that chlorine radicals react with azo dyes to generate halogenated organic compounds under high content of Cl^- (>10 mM), which would promote the degradation of azo dyes [37–39]. However, the influences of Cl^- at high contents (>100 mM) on the mineralization of organics in HSOW treated by SR-AOPs were less considered in the above studies.

In addition, pH conditions would result in the changes of radical species in SR-AOPs with the presence of Cl^- and further impact the degradation of pollutants. $SO_4^{\bullet-}$ is the dominant radical in SR-AOPs under acidic conditions, which would gradually convert to •OH with the pH increasing to alkaline [40–42] [Eq. (2)]. With the presence of Cl^-, the main reactive oxygen species (ROS) in SR-AOPs under acidic conditions would quickly convert from $SO_4^{\bullet-}$ to $Cl^\bullet$ and $Cl_2^{\bullet-}$, which may partially react with OH^- to generate $ClOH^{\bullet-}$ to further give •OH under alkaline conditions. Therefore, the mineralization rate of organics may be promoted with the pH condition increasing from acidic to alkaline in the presence of Cl^- due to the increase of free radical species based on this hypothesis. Moreover, SO_4^{2-} also widely exists in HSOW and may affect organic compound oxidation by reacting with $Cl^\bullet$ to regenerate $SO_4^{\bullet-}$ [Eq. (4)], which has received less attention.

To illustrate the effects and mechanism of different concentrations of Cl^- on the conversion of free radicals and organic matter mineralization by SR-AOPs under different pH conditions, the azo dye (Orange II) as a model pollutant treated by ultraviolet/sodium persulfate (UV/PDS) was investigated. A series of kinetic experiments were conducted to explore the effects of various factors including PDS dosages (0–20 mM), pH (3–10), Cl^- contents (0–1,000 mM), and SO_4^{2-} contents (0–100 mM) on decolorization rate and mineralization rate of Orange II (OrgII). The mechanism of competitive absorbance at 254 nm of OrgII and halogenated intermediate to PDS was proposed based on the observation of UV-VIS absorbance with reaction processing. The transformation of $SO_4^{\bullet-}$ to •OH with Cl^- at 100 mM or without Cl^- was proposed based on electron paramagnetic resonance (EPR) analysis and OrgII mineralization under different pH conditions. Gas chromatography-mass spectrometry (GC-MS) was applied to track the OrgII degradation process and the formation of halogenated intermediate.

2. Materials and methods

2.1. Materials

Sodium persulfate ($Na_2S_2O_8$, 99%), OrgII ($C_{16}H_{11}N_2NaO_4S$, 99%), sodium chloride (NaCl, 99%) were acquired from Kelong Chemical Co., Ltd., China. Sodium dihydrogen phosphate (NaH_2PO_4, 99%), sodium hydrogen phosphate (Na_2HPO_4, 99%), sulfuric acid (H_2SO_4, 98%), and sodium hydroxide (NaOH, 99%) used to adjust pH were of analytical grade. Ultrapure water (18.2 MΩ/cm) was used for solution preparation.

2.2. Experimental procedures

UV irradiation was conducted with a 14 W low pressure mercury lamp (ZW10D15W-Z212, Northeast Lighting Wholesale Co., Ltd., China) emitting predominantly at 254 nm. The lamp tube with the immersion depth of 10 cm was immersed in a 500 mL conical flask glass reactor. The illumination intensity is 7.572×10^{-4}·Einsteins/L/s measured by iodide–iodate actinometry [44]. The solutions contained a desired concentration of PDS, OrgII, and NaCl. The solution pH conditions were buffered with 6.6 mM phosphate. All the experiments were performed at a stirring rate of 800 rpm and 25°C ± 1°C. Reaction solutions were sampled at different time intervals, and the UV-VIS absorbance and total organic carbon (TOC) were determined. The changes of OrgII content and TOC removal were calculated by C_t/C_0 and $(TOC_0–TOC_t)/TOC_0$, respectively, where C_t and TOC_t represent the OrgII concentration and TOC at time t, and C_0 and TOC_0 are the initial concentration and TOC.

Effects of different $Na_2S_2O_8$ dosages (2.5–20 mM) on OrgII removal were investigated. Effects of various pH conditions at 3, 5, 7, and 10 on OrgII removal were investigated. Effects of different Cl^- contents (0–1,000 mM) under various pH conditions at 3, 5, 7, and 10 on OrgII removal were investigated.

Effects of SO_4^{2-} at different concentrations (50–500 mM) on mineralization and decolorization of OrgII with Cl^- at 100 mM were investigated. All the experiments were carried out in duplicates and the averaged values were presented (Table 1).

2.3. Analytical methods

OrgII concentration was determined by detecting the UV-VIS absorbance at 484 nm using a spectrophotometer (UV-L5S, Shanghai Precision Scientific Instrument Co., Ltd., China). TOC determination was carried out in a TOC analyzer (Shimadzu, Japan). Solution pH values were determined by a pHS-3C meter (Rex, China). The residual concentration of PDS was determined by iodometric spectrophotometric [45]. According to the United States Environmental Protection Agency N,N-diethyl-1,4-phenylenediamine (DPD) method. the concentration of free chlorine was determined by spectrophotometric method with DPD colorimetry. The produced reactive species in UV/PDS system were identified on an EPR spectrometer. 5,5-dimethyl-1-pyrroline N-oxide (DMPO) was used as the capturing agent of $SO_4^{\bullet-}$ and $^{\bullet}OH$ for EPR analysis. Degradation intermediates were analyzed by a GC-MS (Agilent 5975 MSD, Agilent, America). The details are indicated in Supporting information S1.

3. Results and discussion

3.1. Effects of PDS dosages on OrgII removal

As shown in Fig. 1a, the OrgII decolorization rate exceeded 95% in 60 min in treatments with PDS dosage ranging from 5 to 20 mM, and the observed first-order decolorization rate constant (k_{obs}) presented a positive correlation with the initial PDS concentration. The OrgII degradation kinetics by UV/PDS were well fitted to pseudo-first-order reaction rate law (Fig. S1). The TOC removal rates were around 20% at 240 min with PDS dosage at 2.5, 5.0, and 7.5 mM, and then reached 97.66% with PDS dosage at 10 and 20 mM (Fig. 1b). The rapid increase in TOC removal rate at PDS doses from 7.5 to 10 mM at 240 min was attributed to the following aspects. The initial absorption at 254 nm of OrgII (0.1 mM, 0.746) was much higher than PDS (10 mM, 0.189) (Fig. 1c and d) resulting in a strong competitive absorbance of ultraviolet light by OrgII at the initial stage of the reaction. However, more ultraviolet light can be utilized by PDS to generate $SO_4^{\bullet-}$ to mineralize intermediate products with reaction processing to more than 60 min due to the complete decolorization of OrgII and less decrease of PDS, especially when higher dosages of PDS were used. Moreover, the produced ROS would firstly oxidize and decompose OrgII

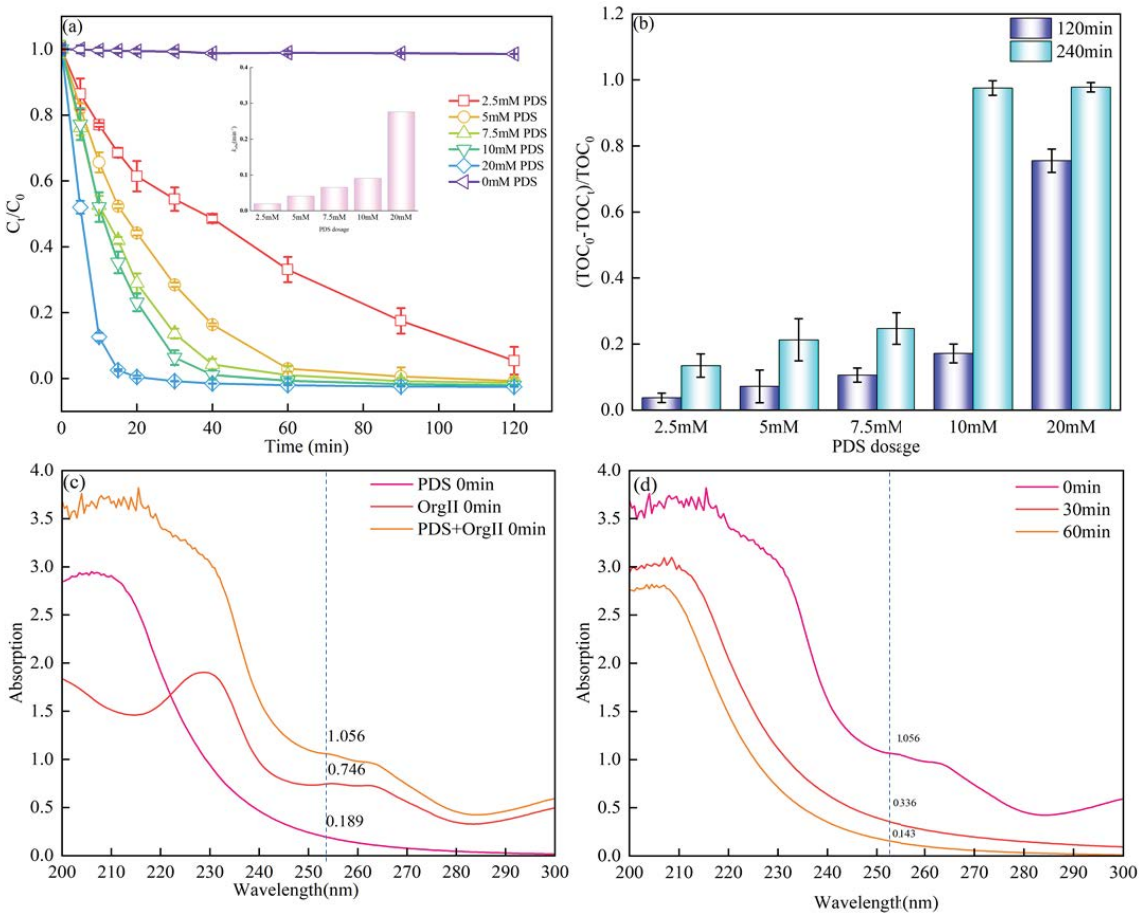

Fig. 1. (a) OrgII decolorization and the observed first-order decolorization rate constant, (b) TOC removal under various PDS dosages, (c) the initial absorption value of OrgII and PDS, and (d) the absorbance value without Cl^-. Reaction conditions: T = 25°C ± 1°C, $[OrgII]_0$ = 0.1 mM, pH = 3.

into small molecular organics, and then a complete mineralization process would occur [46,47]. Besides, the scavenging effects of PDS with dosage increase on $SO_4^{\bullet-}$ were much less than those of H_2O_2 on $^{\bullet}OH$ (2.7×10^7 M/s) [17], which should be due to the relatively slow reaction rate (6.1×10^5 M/s) between $S_2O_8^{2-}$ and $SO_4^{\bullet-}$ [34]. Therefore, considering that higher concentrations of PDS cannot significantly promote mineralization, PDS dosage at 10 mM was used for the subsequent OrgII degradation experiments by UV/PDS.

3.2. Effects of pH conditions on OrgII removal

Compared with OrgII decolorization processes in 10 min, the decolorization rates were close (>90%) after 30 min reaction (Fig. 2a). The highest mineralization rate was only 23.8% in 120 min with pH ranging from 3 to 10. The mineralization rate could reach more than 95% at pH 3 to 7 after 240 min, but was only 80% at pH 10 (Fig. 2b). $^{\bullet}OH$ has lower redox potential than $SO_4^{\bullet-}$ under alkaline conditions, which may decrease the mineralization of organic compounds [48]. In addition, the mineralization of organics into carbon dioxide (CO_2) may introduce the bicarbonate ions (HCO_3^-) and carbonate ions (CO_3^{2-}) into the UV/PDS system at pH 7 and pH 10, and then inhibit further mineralization process of OrgII due to scavenging effects of HCO_3^- and CO_3^{2-} on $SO_4^{\bullet-}$ and $^{\bullet}OH$ [49]. Compared to the treatment at pH 3, the amounts of PDS consumption were enhanced at pH 10 (Fig. 2c). In UV/PDS system, $SO_4^{\bullet-}$ was the dominant ROS under acidic conditions, but $^{\bullet}OH$ would become the main ROS under alkaline conditions due to the quick reaction between $SO_4^{\bullet-}$ and OH^- [Eq. (2)] to produce $^{\bullet}OH$ [50]. The much higher reaction rate constant between $^{\bullet}OH$ and $S_2O_8^{2-}$ ($k = 1.4 \times 10^7$ M/s) [Eq. (6)] than that between $SO_4^{\bullet-}$ and $S_2O_8^{2-}$ ($k = 6.3 \times 10^5$ M/s) [Eq. (7)] [51] may increase scavenging effects of PDS on ROS, and thus the consumption of PDS increased with pH from 3 to 10 (Fig. 2c).

$$S_2O_8^{2-} + {}^{\bullet}OH \rightarrow S_2O_8^{\bullet-} + OH^- \qquad 1.4 \times 10^7 \text{ M/s} \tag{6}$$

$$S_2O_8^{2-} + SO_4^{\bullet-} \rightarrow S_2O_8^{\bullet-} + SO_4^{2-} \qquad 6.3 \times 10^5 \text{ M/s} \tag{7}$$

3.3. Effects of Cl^- contents on OrgII removal

OrgII decolorization rates varied under different Cl^- contents within 30 min, but the final decolorization rates were close (>90%) after 40 min of reaction (Fig. 3a). k_{obs} for OrgII decolorization were increased from 0.0484 to 0.1192 min^{-1} with Cl^- concentration increasing from 50 to 1,000 mM, although the k_{obs} under Cl^- contents ranging from 50 to 500 mM were lower than that in control without Cl^- addition

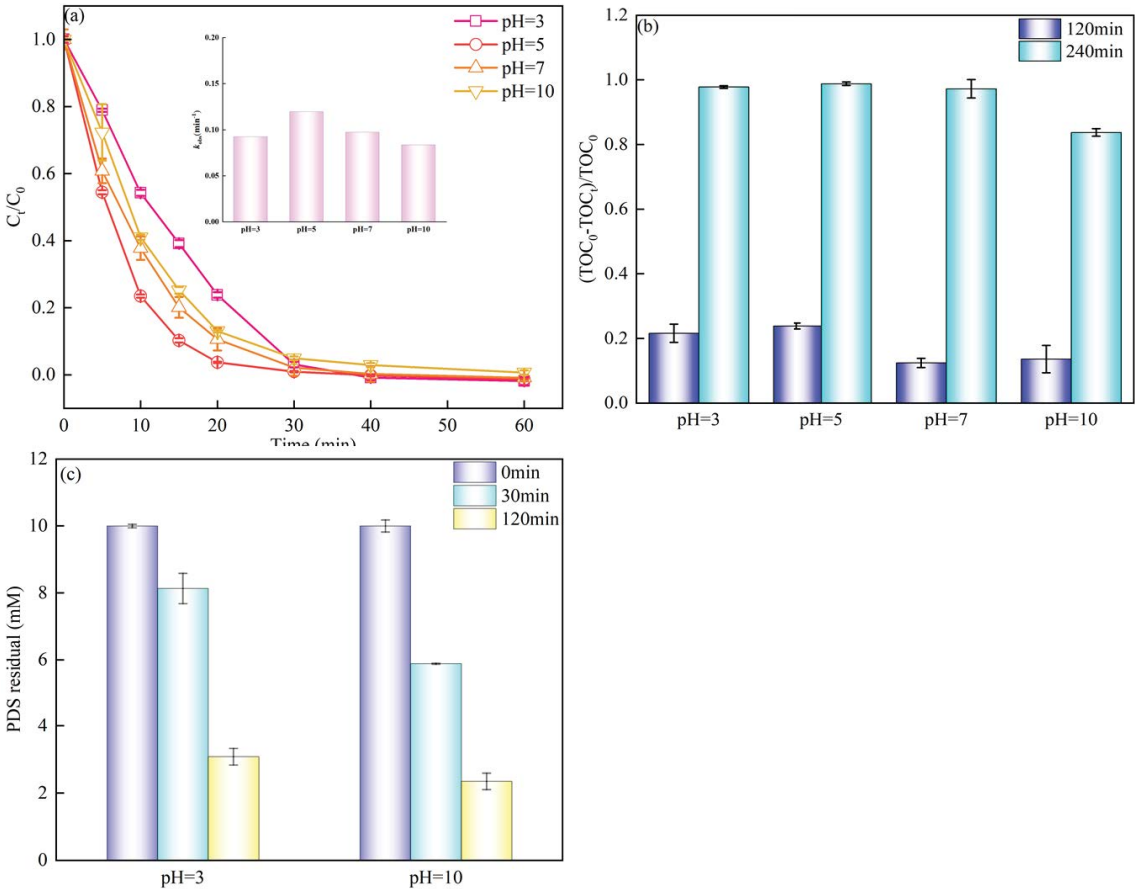

Fig. 2. (a) OrgII decolorization and the observed first-order decolorization rate constant, (b) TOC removal under various pH conditions, and (c) PDS remaining. Reaction conditions: $T = 25°C \pm 1°C$, $[OrgII]_0 = 0.1$ mM, $[PDS]_0 = 10$ mM.

(Fig. 3a). However, the mineralization of OrgII were significantly inhibited (about 70%) in the presence of Cl^- (Fig. 3b). $SO_4^{\bullet-}$ would react with Cl^- to generate $Cl^\bullet$ to further produce $Cl_2^{\bullet-}$ [Eqs. (3) and (5)]. $Cl_2^{\bullet-}$ can quickly react with some unsaturated organic compounds via single electron transfer or hydrogen extraction reaction with the second-order reaction rate constants as high as 10^8~10^9 M/s [52], which can slightly promote the decolorization of OrgII (Fig. 3a). In addition, free chlorines (Cl_2 and HClO) produced by possible reactions [Eqs. (8)–(10)] were determined in contents ranging from 20 to 50 mg/L during the reaction from 30 to 120 min (Fig. 3e) in UV/PDS with Cl^- at 200 and 500 mM under pH 3. Notably, the significant inhibition of OrgII mineralization in the presence of Cl^- revealed that $Cl_2^{\bullet-}$ and free chlorines could not completely oxidize and mineralize OrgII, which was different from the complete mineralization of OrgII by $SO_4^{\bullet-}$. Compared to the treatment without Cl^-, the amounts of PDS consumption were enhanced in the first 30 min, but then were inhibited in 30–120 min in the presence of Cl^- at 200 and 500 mM (Fig. 3c). $SO_4^{\bullet-}$ generated by UV/PDS would quickly react with Cl^- to generate $Cl^\bullet$ and then $Cl_2^{\bullet-}$ [Eqs. (3) and (5)]. The higher reaction rate constants between $Cl^\bullet$ and PDS (8.8×10^6 M/s) [Eq. (11)] [53] than $SO_4^{\bullet-}$ and PDS (6.5×10^5 M/s) [Eq. (7)] [51] would increase the decomposition of PDS (Fig. 3c) in the first 30 min. However, the higher absorption at 254 nm of reaction solutions with 200 mM Cl^- (0.458) than without Cl^- (0.143) after 60 min (Fig. 3d) indicated a higher absorption caused by chlorinated intermediate products, which would reduce the absorbance of ultraviolet light by PDS and further inhibit the mineralization of OrgII.

The effects of Cl^- on the specific organic pollutant removal and total organic compounds removal (mineralization degree) by $SO_4^{\bullet-}$-based AOPs (such as UV/PDS, UV/PMS, and M^{n+1}/PDS) would be quite different. Therefore, this study paid more attention to removing the total organic compound. The effects of varying pH conditions on OrgII degradation with Cl^- at different contents were further investigated.

$$Cl_2^{\bullet-} + Cl_2^{\bullet-} \rightarrow Cl_2 + 2Cl^- \qquad 8.3 \times 10^8 \text{ M/s} \qquad (8)$$

$$Cl^\bullet + Cl^\bullet \rightarrow Cl_2 \qquad 1.0 \times 10^8 \text{ M/s} \qquad (9)$$

$$Cl_2 + H_2O \rightarrow HOCl + H^+ + Cl^- \qquad 15 \text{ M/s} \qquad (10)$$

$$Cl^\bullet + S_2O_8^{2-} \rightarrow \text{products} \qquad 8.8 \times 10^6 \text{ M/s} \qquad (11)$$

3.4. Effects of Cl^- contents on OrgII removal under various pH conditions

OrgII mineralization processes were all significantly inhibited, while OrgII decolorization processes were only slightly influenced in the presence of Cl^- at 200, 500, and 1,000 mM under different pH conditions ranging from 3 to 10 (Fig. S2). However, elevating pH from 3 to 10 promoted k_{obs} of OrgII decolorization under different Cl^- contents (200, 500, and 1,000 mM) within 30 min, although the final decolorization rates were close (>90%) after 60 min of reaction (Fig. 4a–c). In addition, elevating the pH from 3 to 10

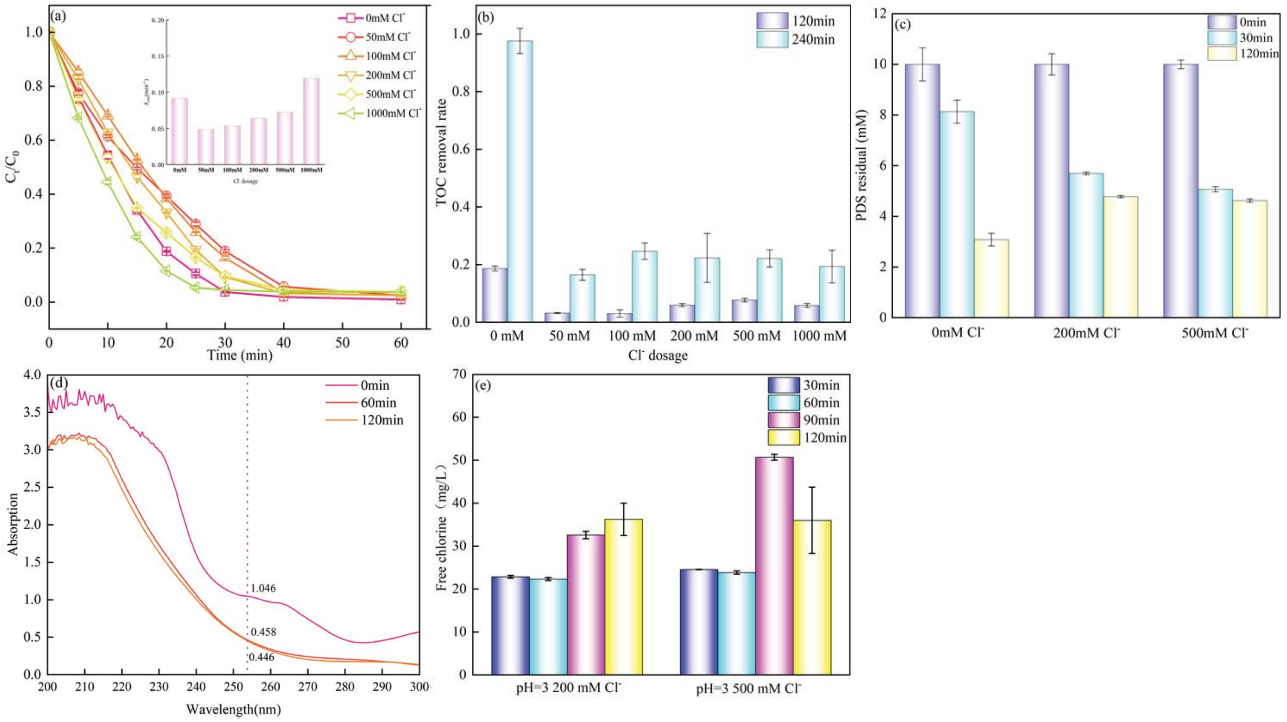

Fig. 3. (a) OrgII decolorization and the observed first-order decolorization rate constant, (b) TOC removal under various Cl^- concentrations, (c) PDS dosage, (d) the absorbance value with Cl^- at 200 mM, and (e) the generation of free chlorine. Reaction conditions: T = 25°C ± 1°C, $[OrgII]_0$ = 0.1 mM, $[PDS]_0$ = 10 mM, pH = 3.

greatly enhanced the decomposition of PDS after 30 min with Cl^- at 200 mM, but inhibited the decomposition of PDS with Cl^- at 500 mM (Fig. 4e).

Elevating the pH from 3 to 10 in treatments with Cl^- at 200 mM can significantly enhance the TOC removal rate by 46% from 22% to 68% (Fig. 4d). $^{\bullet}OH$ would become the main ROS in SR-AOPs due to the reaction between $SO_4^{\bullet-}$ and OH^- [Eq. (2)] when the pH was higher than 9 [54]. However, the conversion of $SO_4^{\bullet-}$ to $^{\bullet}OH$ would occur under pH even less than 6 with the presence of Cl^- (1 mM) in SR-AOPs [55], since $Cl^{\bullet}$ and $Cl_2^{\bullet-}$ generated via the reactions [Eqs. (3) and (5)] would react with H_2O to form $ClOH^{\bullet-}$ [Eqs. (12) and (13)] to further produce $^{\bullet}OH$ [Eq. (16)]. At the same time, $Cl^{\bullet}$ and $Cl_2^{\bullet-}$ would also react with OH^- to form $ClOH^{\bullet-}$ [Eqs. (14) and (15)] to further give $^{\bullet}OH$ under alkaline conditions. Additionally, $S_2O_8^{\bullet-}$ generated by $SO_4^{\bullet-}$ and $Cl^{\bullet}$ reacting with PDS [Eqs. (7) and (11)] would react with chlorinated organic compounds to result in dichlorination [56,57], which would promote the mineralization of intermediate products. In addition, free chlorines (Cl_2 and HClO) produced by possible reactions [Eqs. (8)–(10)] were determined in contents ranging from 20 to 50 mg/L during the reaction from 30 to 120 min (Fig. 4f) in UV/PDS with Cl^- at 200 and 500 mM under both pH 3 and pH 10. The high contents of free chlorines (Cl_2 and HClO) would also inhibit mineralization process.

However, the TOC removal rates increased slightly (less than 20%) with Cl^- at high concentrations (500 and 1,000 mM) with pH increasing from 3 to 10. The possible reasons for less TOC removal under high contents of Cl^- are as follows. More $SO_4^{\bullet-}$ would react with Cl^- to give $Cl^{\bullet}$ and $Cl_2^{\bullet-}$ [Eqs. (3) and (5)], rather than with OH^- to give $^{\bullet}OH$ [Eq. (2)]. More chlorinated products would be produced and compete with PDS to absorb ultraviolet light, which further inhibited the UV activation of PDS and the mineralization process. Moreover, the reaction between Cl^- and $^{\bullet}OH$ would also be favored to give $ClOH^{\bullet-}$ [Eq. (17)] to further reduce the steady-state concentration of $^{\bullet}OH$. The high

Thus, elevating pH value can significantly resist the inhibition of Cl^- at low concentration (200 mM) on OrgII mineralization in UV/PDS system, but the anti-inhibition effects were attenuated under conditions with Cl^- at high concentrations (500 and 1,000 mM).

$$Cl^{\bullet} + H_2O \rightarrow ClOH^{\bullet-} + H^+ \qquad 2.5 \times 10^5\ M/s \qquad (12)$$

$$Cl_2^{\bullet-} + H_2O \rightarrow ClOH^{\bullet-} + H^+ + Cl^- \qquad 1.3 \times 10^3\ M/s \qquad (13)$$

$$Cl^{\bullet} + OH^- \rightarrow ClOH^{\bullet-} \qquad 1.8 \times 10^{10}\ M/s \qquad (14)$$

$$Cl_2^{\bullet-} + OH^- \rightarrow ClOH^{\bullet-} + Cl^- \qquad 4.3 \times 10^9\ M/s \qquad (15)$$

$$ClOH^{\bullet-} \rightarrow {}^{\bullet}OH + Cl^- \qquad 6.1 \times 10^9\ s \qquad (16)$$

$$^{\bullet}OH + Cl^- \rightarrow ClOH^{\bullet-} \qquad 4.3 \times 10^9\ M/s \qquad (17)$$

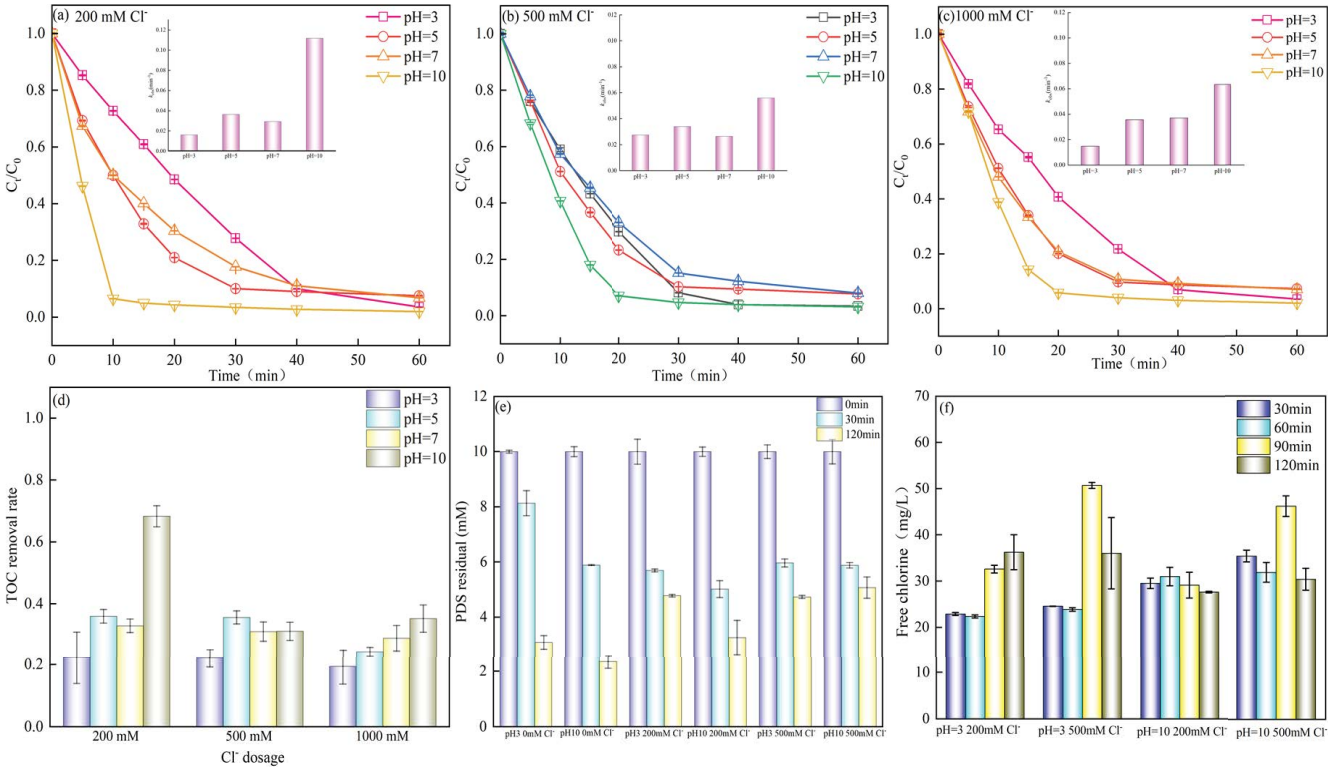

Fig. 4. Effect of various pH conditions on decolorization rate and the observed first-order decolorization rate constant in treatments with Cl^- at (a) 200 mM, (b) 500 mM, (c) 1,000 mM, on (d) TOC removal, (e) PDS dosage, and (f) the generation of free chlorine. Reaction conditions: T = 25°C ± 1°C, $[OrgII]_0$ = 0.1 mM, $[PDS]_0$ = 10 mM.

3.5. Effects of SO_4^{2-} contents on OrgII removal with Cl^- at 100 mM

Effects of SO_4^{2-} at different concentrations (50–500 mM) on mineralization and decolorization of OrgII in the UV/PDS process with Cl^- at 100 mM were shown in Fig. 5. The final decolorization rates and decolorization rates of OrgII were close among treatments under various SO_4^{2-} concentrations (Fig. 5a). The mineralization rates were promoted with SO_4^{2-} concentration increasing from 0 to 100 mM (Fig. 5b), which should be related to the reaction between SO_4^{2-} and $Cl^•$ to regenerate $SO_4^{•-}$ [Eq. (4)] to alleviate the inhibitory effect of Cl^- on TOC removal. However, with SO_4^{2-} concentration increasing from 100 to 500 mM, $SO_4^{•-}$ redox potential would decrease at a high concentration of SO_4^{2-} (>100 mM) [58], which resulted in the decrease of OrgII mineralization. The increase of PDS consumption with SO_4^{2-} addition (Fig. 5c) also supported that less chlorinated intermediates were produced to compete with PDS to absorb ultraviolet light, which indicated that less chlorine radicals ($Cl^•$ and $Cl_2^{•-}$) were generated.

3.6. EPR analysis of $SO_4^{•-}$ and $^•OH$ in the presence of Cl^- in UV/PDS system

The $SO_4^{•-}$ and $^•OH$ accumulation after 5 min in UV/PDS system under pH 3 (without Cl^- and with Cl^- at 100 mM) and pH 10 (without Cl^- and with Cl^- at 100 mM) were compared by EPR analysis with DMPO as the spin trap agent (Fig. 6). The results clearly showed the coexistence of both DMPO-$SO_4^{•-}$ and DMPO-$^•OH$ all the treatments (Fig. 6a). Although DMPO-$^•OH$ showed stronger signals than DMPO-$SO_4^{•-}$ in all the treatments, it did not mean that the concentration of $SO_4^{•-}$ was lower than that of $^•OH$ since the intensities of DMPO-$SO_4^{•-}$ and DMPO-$^•OH$ are not directly related to the concentration $SO_4^{•-}$ and $^•OH$ [59]. The cumulative concentration of DMPO-$SO_4^{•-}$/$^•OH$ without Cl^- or with Cl^- at 100 mM under pH 3 was higher than those under pH 10 (Fig. 6b). Theoretically, the protonation of DMPO (pKa = 2.47) under acidic condition at pH 3 would make it easier for DMPO to capture $SO_4^{•-}$, but DMPO might be negatively charged under alkaline condition at pH 10 to weaken the capture ability to $SO_4^{•-}$. Thus, the stronger ability to capture $SO_4^{•-}$ by DMPO under acidic conditions than alkaline conditions would contribute to the higher cumulative concentration of DMPO-$SO_4^{•-}$/$^•OH$ under pH 3 than pH 10. The cumulative concentration of DMPO-$^•OH$/$SO_4^{•-}$ under pH 3 without Cl^- was slightly higher than that with Cl^- at 100 mM, which illustrated the competitive reaction of Cl^- and DMPO toward $SO_4^{•-}$. The signal of DMPO-$SO_4^{•-}$ was difficult to observe with Cl^- at 100 mM under pH 10 compared to that without Cl^- (Fig. 6a), which was consistent with that more $SO_4^{•-}$ were converted to $^•OH$ in the presence of

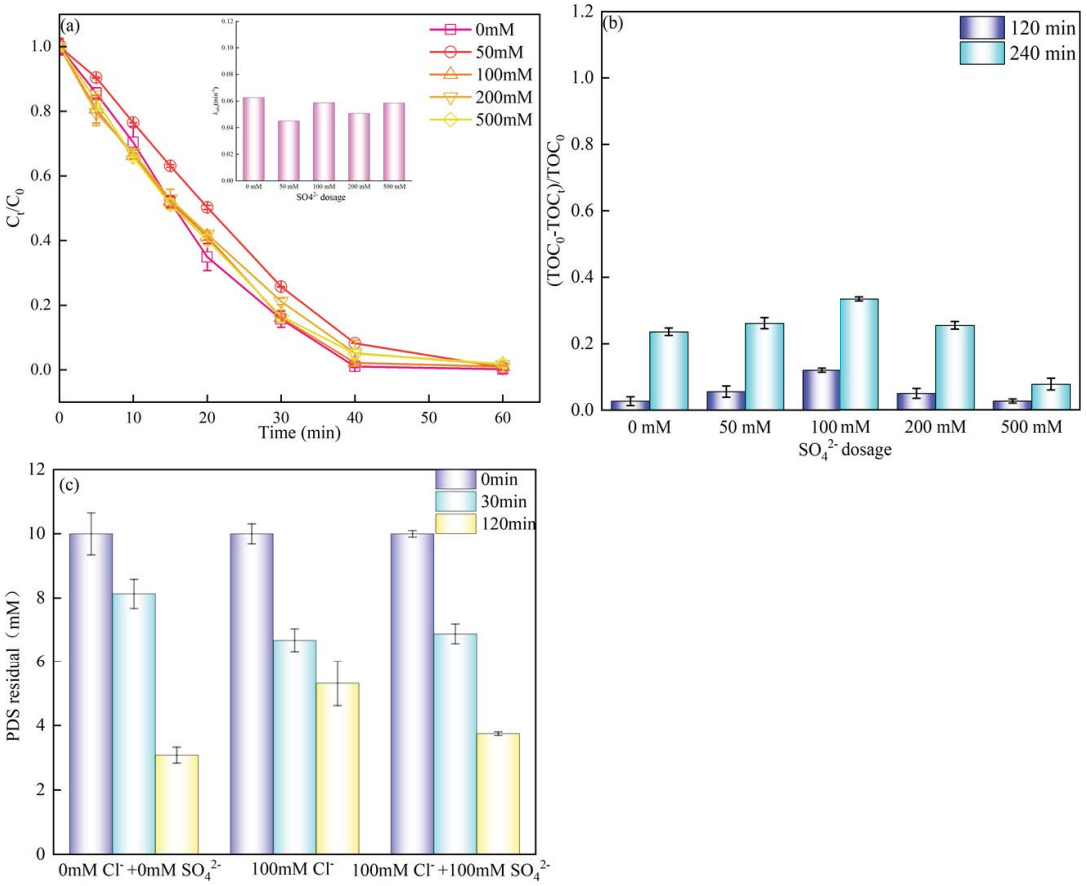

Fig. 5. (a) OrgII decolorization and the observed first-order decolorization rate constant, (b) TOC removal under various SO_4^{2-} concentrations, and (c) PDS dosage. Reaction conditions: T = 25°C ± 1°C, $[OrgII]_0$ = 0.1 mM, $[PDS]_0$ = 10 mM, $[Cl^-]$ = 100 mM.

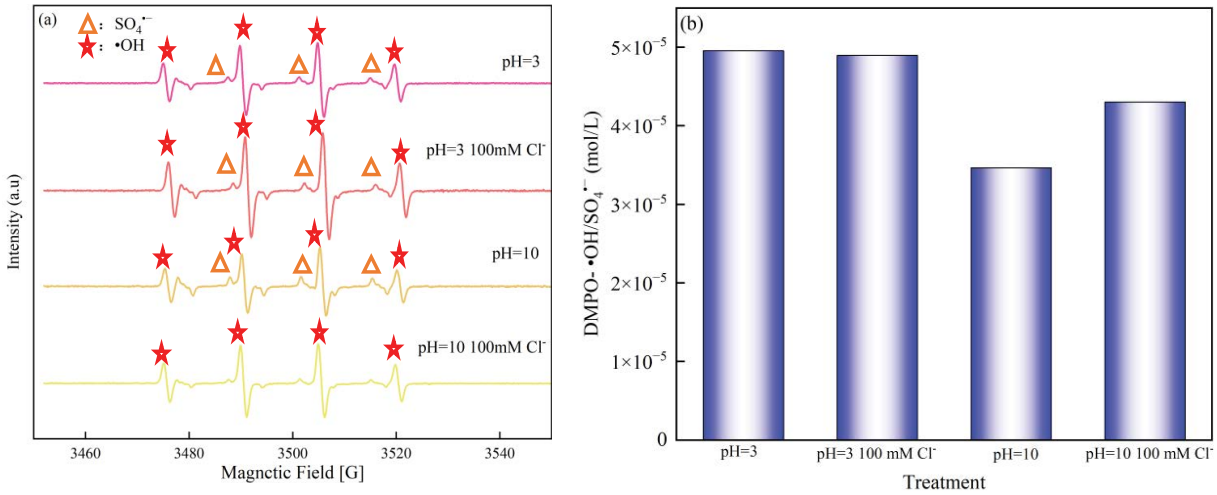

Fig. 6. EPR analysis of $SO_4^{\bullet-}$ and •OH in UV/PDS system captured by DMPO under pH 3 (without Cl^-, with Cl^- at 100 mM) and pH 10 (without Cl^-, with Cl^- at 100 mM): (a) EPR spectrum of DMPO-•OH and DMPO-$SO_4^{\bullet-}$, (b) quantitively analysis of DMPO-•OH and DMPO-$SO_4^{\bullet-}$. Test conditions: DMPO = 100 mM, $[PDS]_0$ = 10 mM, OrgII = 0.1 mM, reaction time = 5 min.

Cl^- [Eqs. (3), (5), (11)–(16)]. Moreover, the higher cumulative concentration of DMPO-•OH/$SO_4^{\bullet-}$ under pH 10 with Cl^- at 100 mM also indicated that •OH was more easily captured than $SO_4^{\bullet-}$ by DMPO under alkaline condition (Fig. 6b).

3.7. Possible degradation way of OrgII in UV/PDS process

$SO_4^{\bullet-}$ as the main ROS produced in UV/PDS process would react with organics through electron transfer, addition, and hydrogen extraction reactions [26]. During the degradation process, the azo bond (–N=N–) of OrgII would be first attacked by $SO_4^{\bullet-}$ (Fig. S3), resulting in the decolorization of dye and the formation of aromatic intermediates, which would be further oxidized to CO_2 and H_2O. However, In the presence of Cl^-, chlorine radicals ($Cl^\bullet$ and $Cl_2^{\bullet-}$) would also participate in the degradation of OrgII to form chlorinated products through electrophilic substitution, which would attack these intermediates to produce more chlorinated by-products and unexpected ring-opening intermediate. The conversion of $SO_4^{\bullet-}$, $Cl^\bullet$, $Cl_2^{\bullet-}$, and $ClOH^{\bullet-}$ to •OH would occur at pH 5 [55], which may promote the mineralization of aromatic intermediates. Therefore, according to the degradation by-products identified by GC-MS (Figs. S4 and S5), the main intermediates way in UV/PDS with Cl^- at 100 under pH 3 and 10 was proposed (Fig. 7).

In control group without Cl^- under pH 3, the main intermediates of OrgII in UV/PDS degradation process were aromatic compounds (P1–P5). Aromatic compounds (P2, P6), carboxylic acids (P11, P12), and chloroalkane (P13) were detected in all treatments with Cl^-. Compared to treatment without Cl^- under pH 3, more intermediates were detected with Cl^- at 100 mM, such as aromatic compounds (P2, P6), long-chain carboxylic acids (P8–P10), short-chain carboxylic acids (P11, P12), and chloroalkane (P13), which should be attributed to the lower oxidation ability of chloride radicals compared to sulfate radicals. Moreover, as mentioned above in Section 3.3 and Fig. S2, these intermediates may cause stronger competition absorption to ultraviolet light to inhibit the mineralization process by UV/PDS. However, long-chain carboxylic acids (P8–P10) could not be detected in the treatment with 100 mM Cl^- and 100 mM SO_4^{2-} under pH 3. In addition, elevating pH from 3 to 10 significantly reduced the variety of carboxylic acids (P8–P10) in UV/PDS degradation process with Cl^- at 100 mM. Therefore, introducing SO_4^{2-} and elevating pH reduced the types of intermediate products, which could be beneficial for PDS to absorb ultraviolet light to promote the mineralization process. Interestingly, although Cl^- showed a great inhibition on OrgII mineralization, only one chlorinated by-product (3-chloro-3-methylpentane) was detected in UV/PDS system, which was much less than those in UV/H_2O_2 system in previous study [17]. Much less TOC removal and chlorinated by-product in UV/PDS than UV/H_2O_2 may be related to that much more free chlorine generated in UV/PDS (20–50 mg/L) (Fig. S3) than UV/H_2O_2 (0.05–0.8 mg/L) [17] reduced the oxidation capacity of UV/PDS system.

3.8. Cost estimation in real wastewater

Gas field produced water (Yuanba, Sichuan, Cl^- = 30,000 mg/L) and lake water (Chengdu, Sichuan, Cl^- = 50 mg/L) were selected for cost estimation by evaluating the relationship between TOC removal and PDS consumption under pH 3 and 10. As shown in Fig. 8a, the lake water TOC removal was higher than gas field produced water TOC removal under pH 3 and 10. The PDS decomposition in gas field produced water was higher than lake water under pH 3 and 10 (Fig. 8b). It can be obtained that the PDS required to remove 1 mg of TOC under pH 3 and 10 from the lake water were 3.72, 3.36, 6.92, and 4.8 mM under pH 3 and 10 in gas field produced water, respectively.

The TOC in gas field water and lake water are 500 and 60 mg/L, respectively. It is assumed that the TOC removal rate of industrial wastewater is 50% to meet the standard. The PDS market price is 714 USD/t. The reagent cost of UV/PDS process for treating gas fields produced water is much

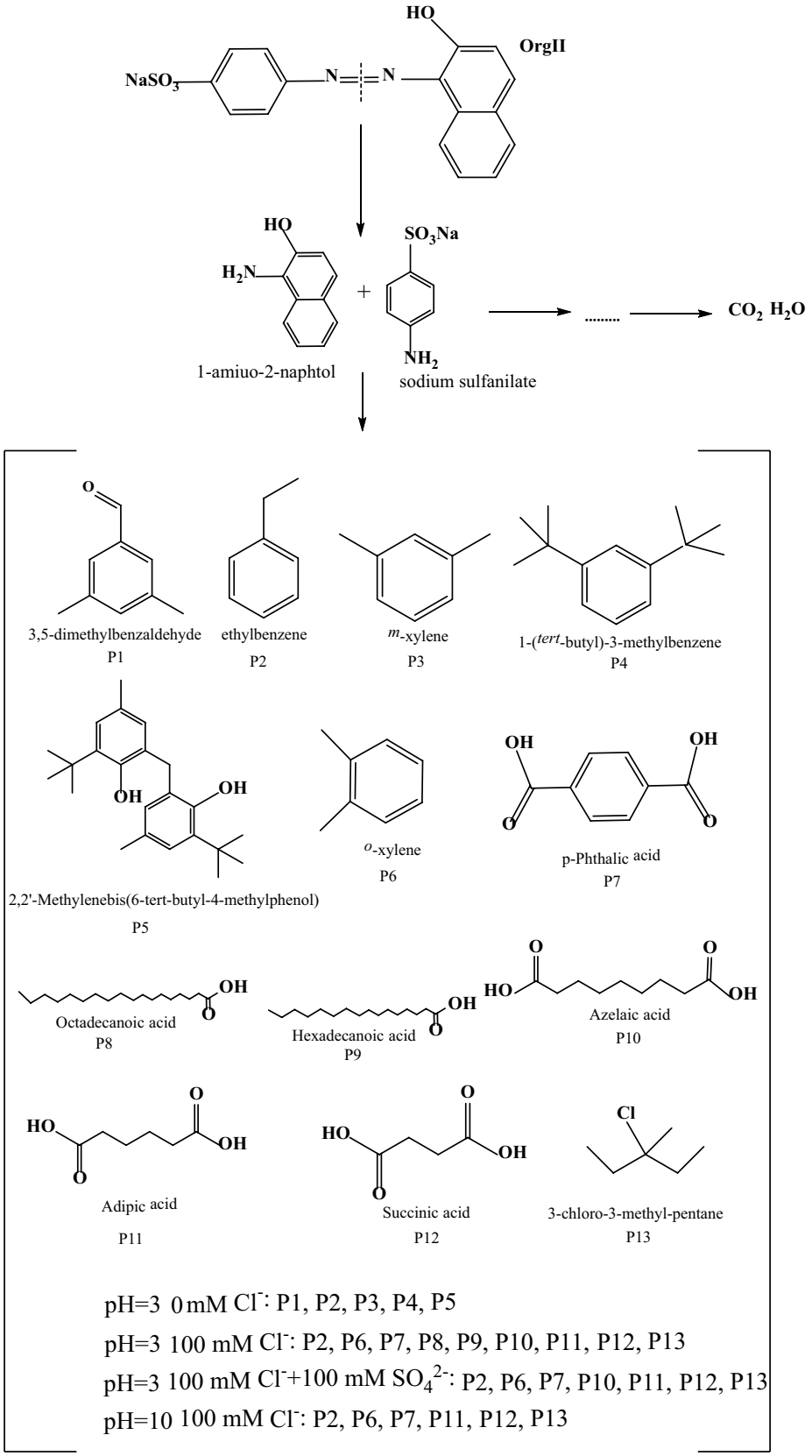

Fig. 7. Main intermediates during OrgII degradation by UV/PDS under various conditions with and without Cl^- at 100 mM under pH 3, with Cl^- at 100 mM and SO_4^{2-} at 100 mM under pH 3, and with Cl^- at 100 mM under pH 10. Reaction conditions: T = 25°C ± 1°C, $[OrgII]_0$ = 0.1 mM, $[PDS]_0$ = 10 mM.

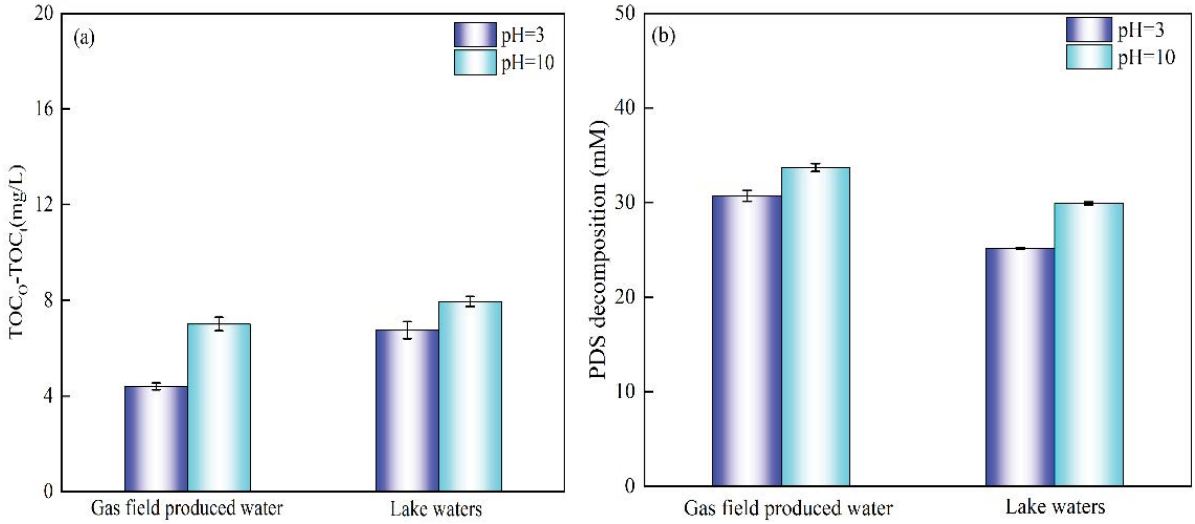

Fig. 8. Effect of various pH conditions with different aqueous matrix on (a) TOC removal and (b) PDS decomposition. Reaction conditions: T = 25°C ± 1°C, $[PDS]_0$ = 50 mM, reaction time = 120 min.

Table 1
Partial reactions and rate constants in SR-AOPs in the presence of Cl^-

Reaction	Rate constant (M/s)	Number
$S_2O_8^{2-} \xrightarrow{UV} 2SO_4^{\bullet-}$	$r = 2FI_0f_{parent}(1-10^{-(\alpha(\lambda)+\varepsilon(\lambda)C)l})$, $\Phi = 0.7$ [43]	(1)
$SO_4^{\bullet-} + OH^- \rightarrow SO_4^{2-} + {}^{\bullet}OH$	7×10^7 M/s	(2)
$SO_4^{\bullet-} + Cl^- \rightarrow SO_4^{2-} + Cl^{\bullet}$	2.7×10^8 M/s	(3)
$SO_4^{2-} + Cl^{\bullet} \rightarrow SO_4^{\bullet-} + Cl^-$	2.5×10^8 M/s	(4)
$Cl^{\bullet} + Cl^- \rightarrow Cl_2^{\bullet-}$	8.5×10^9 M/s	(5)

higher (about 219 USD/t) than lake water (about 18 USD/t). Therefore, the UV/PDS process is not suitable to deal with industrial wastewater, such as gas fields produced water.

4. Conclusion

Effects of pH and SO_4^{2-} combined with Cl^- on the removal of azo dye OrgII treated by UV/PDS were investigated. Adding Cl^- barely impacted the final decolorization rates of OrgII, but significantly inhibited the mineralization, which was attributed to that the produced chlorine radicals ($Cl^{\bullet}$ and $Cl_2^{\bullet-}$) and free chlorines (Cl_2 and HClO) cannot decompose OrgII completely and the chlorinated intermediate products competed with PDS to absorb ultraviolet light. Elevating the pH from 3 to 10 promoted the TOC removal rates significantly with Cl^- at 200 mM (by 46%) but slightly with Cl^- at 1,000 mM (by 16%) since the transformation of $SO_4^{\bullet-}$, $Cl^{\bullet}$, and $Cl_2^{\bullet-}$ to $^{\bullet}OH$ under various Cl^- concentrations would be different, and $S_2O_8^{\bullet-}$ generated from the reaction between $^{\bullet}OH$ and PDS was also capable of dehalogenation. Adding SO_4^{2-} at 50 and 100 mM can resist the inhibition of Cl^- (100 mM) on OrgII mineralization since the reaction between SO_4^{2-} and $Cl^{\bullet}$ to regenerate $SO_4^{\bullet-}$. The increase of PDS consumption with SO_4^{2-} addition also supported that less chlorine radicals ($Cl^{\bullet}$ and $Cl_2^{\bullet-}$) were generated to produce less chlorinated intermediates to compete with PDS to absorb ultraviolet light. However, SO_4^{2-} at high concentration (200 and 500 mM) may reduce the redox potential of $SO_4^{\bullet-}$ to further decrease the TOC removal rate. The results reveal the complex effects of Cl^- contents under different pH conditions and various SO_4^{2-} contents on the removal of organic pollutants by SR-AOPs, which provides better strategies to remove the organic compounds in HSOW treatment by SR-AOPs.

Credit author statement

Bing Yang: Investigation, Visualization, Writing-review and editing. Xiangfu Huang: Investigation, Visualization, Writing-original draft. Yucheng Liu: Resources, Funding acquisition, Project administration. Mi Zhou: Methodology, Investigation, Software. Wei Jiang: Resources, Methodology. Qinman Li, Qiuping Luo: Investigation, Data curation. Lili Ma: Validation. Lingli Li: Supervision, Writing-review and editing.

Funding

This research was partially supported by the National Natural Science Foundation of China (21707111), the Opening Project of Oil & Gas Field Applied Chemistry Key Laboratory of Sichuan Province (YQKF202119, YQKF202106), Sichuan Science and Technology Support Project (2020JDTD0018), and China Postdoctoral Science Foundation (2021M692263).

Declaration of competing interest

The authors declare that they have no known competing financial interests or personal relationships that could have appeared to influence the work reported in this paper.

Data availability

Data will be made available on request.

References

[1] W. An, J. Zhao, J. Lu, Y. Han, D. Li, Zero-liquid discharge technologies for desulfurization wastewater: a review, J. Environ. Manage., 321 (2022) 115953, doi: 10.1016/j.jenvman.2022.115953.

[2] E. Barbot, N.S. Vidic, K.B. Gregory, R.D. Vidic, Spatial and temporal correlation of water quality parameters of produced waters from Devonian-age shale following hydraulic fracturing, Environ. Sci. Technol., 47 (2013) 2562–2569.

[3] Z. Sun, H. Chen, N. Zhao, Y. Feng, F. Liu, C. Cai, G. Che, L. Yang, Experimental research and engineering application on the treatment of desulfurization wastewater from coal-fired power plants by spray evaporation, J. Water Process Eng., 40 (2021) 101960, doi: 10.1016/j.jwpe.2021.101960.

[4] S. Alzahrani, A.W. Mohammad, Challenges and trends in membrane technology implementation for produced water treatment: a review, J. Water Process Eng., 4 (2014) 107–133.

[5] M.A. Al-Ghouti, M.A. Al-Kaabi, M.Y. Ashfaq, D.A. Da'na, Produced water characteristics, treatment and reuse: a review, J. Water Process Eng., 28 (2019) 222–239.

[6] E. Obotey Ezugbe, S. Rathilal, Membrane technologies in wastewater treatment: a review, Membranes, 10 (2020) 89, doi: 10.3390/membranes10050089.

[7] Y. Suo, Y. Ren, Research on the mechanism of nanofiltration membrane fouling in zero discharge process of high salty wastewater from coal chemical industry, Chem. Eng. Sci., 245 (2021) 116810, doi: 10.1016/j.ces.2021.116810.

[8] F. Zhao, F. Ju, K. Huang, Y. Mao, X. Zhang, H. Ren, T. Zhang, Comprehensive insights into the key components of bacterial assemblages in pharmaceutical wastewater treatment plants, Sci. Total Environ., 651 (2019) 2148–2157.

[9] Z. Wu, J. Fang, Y. Xiang, C. Shang, X. Li, F. Meng, X. Yang, Roles of reactive chlorine species in trimethoprim degradation in the UV/chlorine process: kinetics and transformation pathways, Water Res., 104 (2016) 272–282.

[10] H. Liu, Z. Hou, Y. Li, Y. Lei, Z. Xu, J. Gu, S. Tian, Modeling degradation kinetics of gemfibrozil and naproxen in the UV/chlorine system: roles of reactive species and effects of water matrix, Water Res., 202 (2021) 117445, doi: 10.1016/j.watres.2021.117445.

[11] A. Hassani, P. Eghbali, F. Mahdipour, S. Wacławek, K.-Y.A. Lin, F. Ghanbari, Insights into the synergistic role of photocatalytic activation of peroxymonosulfate by UVA-LED irradiation over $CoFe_2O_4$-rGO nanocomposite towards effective Bisphenol A degradation: performance, mineralization, and activation mechanism, Chem. Eng. J., 453 (2023) 139556, doi: 10.1016/j.cej.2022.139556.

[12] S. Madihi-Bidgoli, S. Asadnezhad, A. Yaghoot-Nezhad, A. Hassani, Azurobine degradation using Fe_2O_3@multi-walled carbon nanotube activated peroxymonosulfate (PMS) under UVA-LED irradiation: performance, mechanism and environmental application, J. Environ. Chem. Eng., 9 (2021) 106660, doi: 10.1016/j.jece.2021.106660.

[13] F. Ghanbari, Q. Wang, A. Hassani, S. Waclawek, J. Rodriguez-Chueca, K.A. Lin, Electrochemical activation of peroxides for treatment of contaminated water with landfill leachate: efficacy, toxicity and biodegradability evaluation, Chemosphere, 279 (2021) 130610, doi: 10.1016/j.chemosphere.2021.130610.

[14] G. Meng, Y. Wang, X. Li, H. Zhang, X. Zhou, Z. Bai, L. Wu, J. Bai, Treatment of landfill leachate evaporation concentrate by a modified electro-Fenton method, Environ. Technol., 43 (2022) 500–513.

[15] H. Liu, Y. Gao, J. Wang, D. Ma, Y. Wang, B. Gao, Q. Yue, X. Xu, The application of UV/O_3 process on ciprofloxacin wastewater containing high salinity: performance and its degradation mechanism, Chemosphere, 276 (2021) 130220, doi: 10.1016/j.chemosphere.2021.130220.

[16] Y. Yang, J.J. Pignatello, J. Ma, W.A. Mitch, Effect of matrix components on UV/H_2O_2 and UV/$S_2O_8^{2-}$ advanced oxidation processes for trace organic degradation in reverse osmosis brines from municipal wastewater reuse facilities, Water Res., 89 (2016) 192–200.

[17] B. Yang, Q. Luo, Q. Li, R. Jia, Y. Liu, X. Huang, M. Zhou, L. Li, Dye mineralization under UV/H_2O_2 promoted by chloride ion at high concentration and the generation of chlorinated byproducts, Sci. Total Environ., 857 (2022) 159453, doi: 10.1016/j.scitotenv.2022.159453.

[18] X. Lai, X.-A. Ning, Y. Zhang, Y. Li, R. Li, J. Chen, S. Wu, Treatment of simulated textile sludge using the Fenton/Cl^- system: the roles of chlorine radicals and superoxide anions on PAHs removal, Environ. Res., 197 (2021) 110997, doi: 10.1016/j.envres.2021.110997.

[19] C.M. Dominguez, A. Romero, D. Lorenzo, A. Santos, Thermally activated persulfate for the chemical oxidation of chlorinated organic compounds in groundwater, J. Environ. Manage., 261 (2020) 110240, doi: 10.1016/j.jenvman.2020.110240.

[20] Z. Li, L. Wang, Y. Liu, Q. Zhao, J. Ma, Unraveling the interaction of hydroxylamine and Fe(III) in Fe(II)/persulfate system: a kinetic and simulating study, Water Res., 168 (2020) 115093, doi: 10.1016/j.watres.2019.115093.

[21] X. Lei, Y. Lei, J.M. Guan, P. Westerho, X. Yang, Kinetics and transformations of diverse dissolved organic matter fractions with sulfate radicals, Environ. Sci. Technol., 56 (2022) 4457–4466.

[22] C. Tan, Y. Dong, D. Fu, N. Gao, J. Ma, X. Liu, Chloramphenicol removal by zero valent iron activated peroxymonosulfate system: kinetics and mechanism of radical generation, Chem. Eng. J., 334 (2018) 1006–1015.

[23] J. Deng, Y. Cheng, Y. Lu, J.C. Crittenden, S. Zhou, N. Gao, J. Li, Mesoporous manganese cobaltite nanocages as effective and reusable heterogeneous peroxymonosulfate activators for carbamazepine degradation, Chem. Eng. J., 330 (2017) 505–517.

[24] L.W. Matzek, K.E. Carter, Sustained persulfate activation using solid iron: kinetics and application to ciprofloxacin degradation, Chem. Eng. J., 307 (2017) 650–660.

[25] C. Liang, I.L. Lee, I.Y. Hsu, C. Liang, Y. Lin, Persulfate oxidation of trichloroethylene with and without iron activation in porous media, Chemosphere, 70 (2008) 426–435.

[26] X. Zeng, Y. Meng, X. Sun, F. Guo, M. Yang, Experimental and theoretical investigation on degradation of enoxacin in aqueous solution by UV-activated persulfate: kinetics, influencing factors and degradation pathways, J. Environ. Chem. Eng., 9 (2021) 106608, doi: 10.1016/j.jece.2021.106608.

[27] Z. Li, W. Qi, Y. Feng, Y. Liu, E. Shehata, J. Long, Degradation mechanisms of oxytetracycline in the environment, J. Integr. Agric., 18 (2019) 1953–1960.

[28] A. Ghauch, A.M. Tuqan, N. Kibbi, Ibuprofen removal by heated persulfate in aqueous solution: a kinetics study, Chem. Eng. J., 197 (2012) 483–492.

[29] K.H. Chan, W. Chu, Degradation of atrazine by cobalt-mediated activation of peroxymonosulfate: different cobalt counter-anions in homogenous process and cobalt oxide catalysts in photolytic heterogeneous process, Water Res., 43 (2009) 2513–2521.

[30] G.P. Anipsitakis, D.D. Dionysiou, M.A. Gonzalez, Cobalt-mediated activation of peroxymonosulfate and sulfate radical attack on phenolic compounds. Implications of chloride ions, Environ. Sci. Technol., 40 (2006) 1000–1007.

[31] Y. Lei, S. Cheng, N. Luo, X. Yang, T. An, rate constants and mechanisms of the reactions of $Cl^•$ and $Cl_2^{•-}$ with trace organic contaminants, Environ. Sci. Technol., 53 (2019) 11170–11182.

[32] Y. Lei, X. Lei, P. Westerhoff, X. Zhang, X. Yang, Reactivity of chlorine radicals ($Cl^•$ and $Cl_2^{•-}$) with dissolved organic matter and the formation of chlorinated byproducts, Environ. Sci. Technol., 55 (2021) 689–699.

[33] K. Hasegawa, P. Neta, Rate constants and mechanisms of reaction of chloride (Cl^{2-}) radicals, J. Phys. Chem., 82 (1978) 854–857.

[34] L. Liu, S. Lin, W. Zhang, U. Farooq, G. Shen, S. Hu, Kinetic and mechanistic investigations of the degradation of

sulfachloropyridazine in heat-activated persulfate oxidation process, Chem. Eng. J., 346 (2018) 515–524.
[35] M. Xu, X. Gu, S. Lu, Z. Miao, X. Zang, X. Wu, Z. Qiu, Q. Sui, Degradation of carbon tetrachloride in thermally activated persulfate system in the presence of formic acid, Front. Environ. Sci. Eng., 10 (2016) 438–446.
[36] Y. Feng, Q. Song, W. Lv, G. Liu, Degradation of ketoprofen by sulfate radical-based advanced oxidation processes: kinetics, mechanisms, and effects of natural water matrices, Chemosphere, 189 (2017) 643–651.
[37] Z. Wang, R. Yuan, Y. Guo, L. Xu, J. Liu, Effects of chloride ions on bleaching of azo dyes by Co^{2+}/oxone regent: kinetic analysis, J. Hazard. Mater., 190 (2011) 1083–1087.
[38] H. Gao, J. Chen, Y. Zhang, X. Zhou, Sulfate radicals induced degradation of triclosan in thermally activated persulfate system, Chem. Eng. J., 306 (2016) 522–530.
[39] Y. Qian, G. Xue, J. Chen, J. Luo, X. Zhou, P. Gao, Q. Wang, Oxidation of cefalexin by thermally activated persulfate: kinetics, products, and antibacterial activity change, J. Hazard. Mater., 354 (2018) 153–160.
[40] C. Liang, Z. Wang, C.J. Bruell, Influence of pH on persulfate oxidation of TCE at ambient temperatures, Chemosphere, 66 (2007) 106–113.
[41] G. Fang, D.D. Dionysiou, Y. Wang, S.R. Al-Abed, D. Zhou, Sulfate radical-based degradation of polychlorinated biphenyls: effects of chloride ion and reaction kinetics, J. Hazard. Mater., 227 (2012) 394–401.
[42] Y. Wu, Y. Yang, Y. Liu, L. Zhang, L. Feng, Modelling study on the effects of chloride on the degradation of bezafibrate and carbamazepine in sulfate radical-based advanced oxidation processes: conversion of reactive radicals, Chem. Eng. J., 358 (2019) 1332–1341.
[43] G. Mark, M.N. Schuchmann, H.-P. Schuchmann, C. von Sonntag, The photolysis of potassium peroxodisulphate in aqueous solution in the presence of *tert*-butanol: a simple actinometer for 254 nm radiation, J. Photochem. Photobiol., A, 55 (1990) 157–168.
[44] R.O. Rahn, M.I. Stefan, J.R. Bolton, E. Goren, P.S. Shaw, K.R. Lykke, Quantum yield of the iodide-iodate chemical actinometer: dependence on wavelength and concentrations, Photochem. Photobiol., 78 (2003) 146–152.
[45] C. Liang, C.F. Huang, N. Mohanty, R.M. Kurakalva, A rapid spectrophotometric determination of persulfate anion in ISCO, Chemosphere, 73 (2008) 1540–1543.
[46] Y. Shih, Y. Li, Y. Huang, Application of UV/persulfate oxidation process for mineralization of 2,2,3,3-tetrafluoro-1-propanol, J. Taiwan Inst. Chem. Eng., 44 (2013) 287–290.
[47] H. Guo, T. Ke, N. Gao, Y. Liu, X. Cheng, Enhanced degradation of aqueous norfloxacin and enrofloxacin by UV-activated persulfate: kinetics, pathways and deactivation, Chem. Eng. J., 316 (2017) 471–480.
[48] J. Wang, S. Wang, Activation of persulfate (PS) and peroxymonosulfate (PMS) and application for the degradation of emerging contaminants, Chem. Eng. J., 334 (2018) 1502–1517.
[49] S. Guo, Q. Wang, C. Luo, J. Yao, Z. Qiu, Q. Li, Hydroxyl radical-based and sulfate radical-based photocatalytic advanced oxidation processes for treatment of refractory organic matter in semi-aerobic aged refuse biofilter effluent arising from treating landfill leachate, Chemosphere, 243 (2020) 125390, doi: 10.1016/j.chemosphere.2019.125390.
[50] H. Zhang, Z. Wang, C. Liu, Y. Guo, N. Shan, C. Meng, L. Sun, Removal of COD from landfill leachate by an electro/Fe^{2+}/peroxydisulfate process, Chem. Eng. J., 250 (2014) 76–82.
[51] T.N. Das, Reactivity and role of $SO_5^{\bullet-}$ radical in aqueous medium chain oxidation of sulfite to sulfate and atmospheric sulfuric acid generation, J. Phys. Chem. A, 105 (2001) 9142–9155.
[52] J. Lee, U. von Gunten, J.H. Kim, Persulfate-based advanced oxidation: critical assessment of opportunities and roadblocks, Environ. Sci. Technol., 54 (2020) 3064–3081.
[53] X.-Y. Yu, Z.-C. Bao, J.R. Barker, Free radical reactions involving $Cl^{\bullet}$, $Cl_2^{\bullet-}$, and $SO_4^{\bullet-}$ in the 248 nm photolysis of aqueous solutions containing $S_2O_8^{2-}$ and Cl^-, J. Phys. Chem. A, 108 (2004) 295–308.
[54] N. Yousefi, S. Pourfadakari, S. Esmaeili, A.A. Babaei, Mineralization of high saline petrochemical wastewater using sonoelectro-activated persulfate: degradation mechanisms and reaction kinetics, Microchem. J., 147 (2019) 1075–1082.
[55] H.V. Lutze, N. Kerlin, T.C. Schmidt, Sulfate radical-based water treatment in presence of chloride: formation of chlorate, inter-conversion of sulfate radicals into hydroxyl radicals and influence of bicarbonate, Water Res., 72 (2015) 349–360.
[56] C. Zhu, F. Zhu, D.D. Dionysiou, D. Zhou, G. Fang, J. Gao, Contribution of alcohol radicals to contaminant degradation in quenching studies of persulfate activation process, Water Res., 139 (2018) 66–73.
[57] C. Zhu, F. Zhu, C. Liu, N. Chen, D. Zhou, G. Fang, J. Gao, Reductive hexachloroethane degradation by $S_2O_8^{\bullet-}$ with thermal activation of persulfate under anaerobic conditions, Environ. Sci. Technol., 52 (2018) 8548–8557.
[58] J. Wang, S. Wang, Effect of inorganic anions on the performance of advanced oxidation processes for degradation of organic contaminants, Chem. Eng. J., 411 (2021) 128392, doi: 10.1016/j.cej.2020.128392.
[59] H. Zhang, C. Xie, L. Chen, J. Duan, F. Li, W. Liu, Different reaction mechanisms of $SO_4^{\bullet-}$ and $^{\bullet}OH$ with organic compound interpreted at molecular orbital level in Co(II)/peroxymonosulfate catalytic activation system, Water Res., 229 (2023) 119392, doi: 10.1016/j.watres.2022.119392.

Supporting information

S1. Experimental conditions of gas chromatography-mass spectrometry analysis

Degradation intermediates of Orange II (OrgII) treated by ultraviolet/sodium persulfate (UV/PDS) process were analyzed by a gas chromatography-mass spectrometry (GC-MS, Agilent 5975 MSD, Agilent, America). Take 20 mL of sample at 30, 60, and 120 min of reaction, and then mix to obtain 60 mL of solution. 60 mL solution was withdrawn and placed into the freezing layer of the refrigerator to freeze solid, and then the moisture was removed by freeze-drying. The dried materials were put into a 2 mL plastic-stoppered vial and then treated with 1 mL of dichloromethane, 0.1 mL of hexamethyldisilane, and 0.05 mL of trimethylchlorosilane. The mixtures were shaken vigorously for about 30 min and then separated by centrifugation for 10 min. Finally, the supernatants were taken out and passed through 0.22 μm organic filter membranes before chromatographic analysis.

The GC-MS analysis conditions were as follows: the initial injection temperature was 40°C and kept for 10 min, and then the temperature was raised to 100°C at 12°C/min. Next, the temperature was raised to 200°C at 5°C/min, and finally raised up to 270°C at 20°C/min and kept for 5 min. The carrier gas was helium, and the flow rate was 1 mL/min.

S2. Pseudo-first-order kinetic fitting of OrgII decolorization

As shown in Fig. S1, OrgII decolorization by UV/PDS could be well fitted with the pseudo-first-order kinetics model, described in Eq. (S1).

$$\ln\left(\frac{C_{t,\mathrm{OrgII}}}{C_{0,\mathrm{OrgII}}}\right) = k_{\mathrm{obs}} \times t \tag{S1}$$

where $C_{t,\mathrm{OrgII}}$ and $C_{0,\mathrm{OrgII}}$ represent the dye concentration at time t and the initial concentration, respectively, and k_{obs} indicates the observed pseudo-first-order reaction rate constant (min^{-1}).

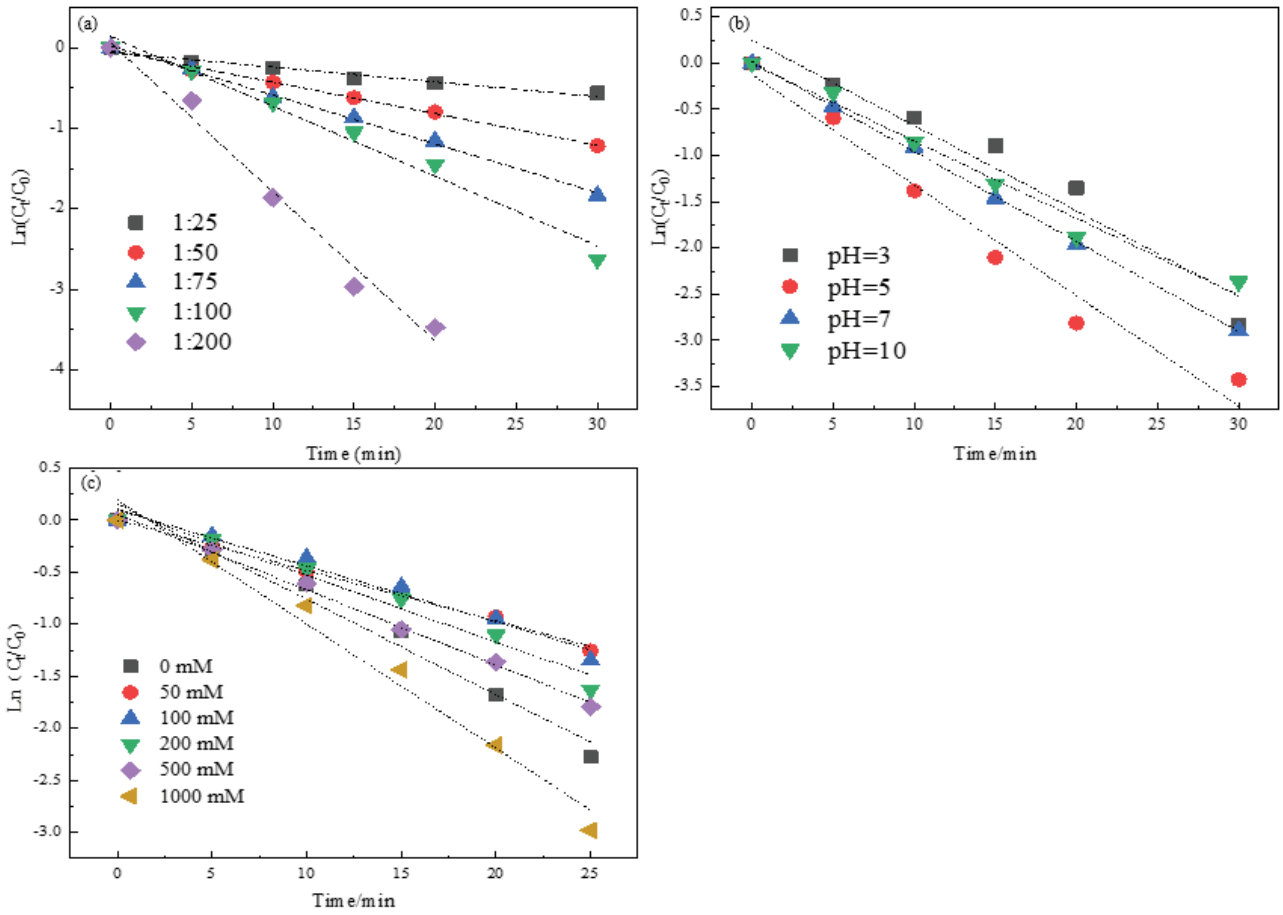

Fig. S1. Pseudo-first-order kinetic model of OrgII decolorization process under (a) different PDS dosages, (b) different pH conditions, and (c) different concentration of Cl^- at pH 3, $[OrgII]_0$ = 0.1 mM, T = 25°C ± 1°C.

S3. Effects of different Cl– concentrations under the same pH condition on OrgII removal

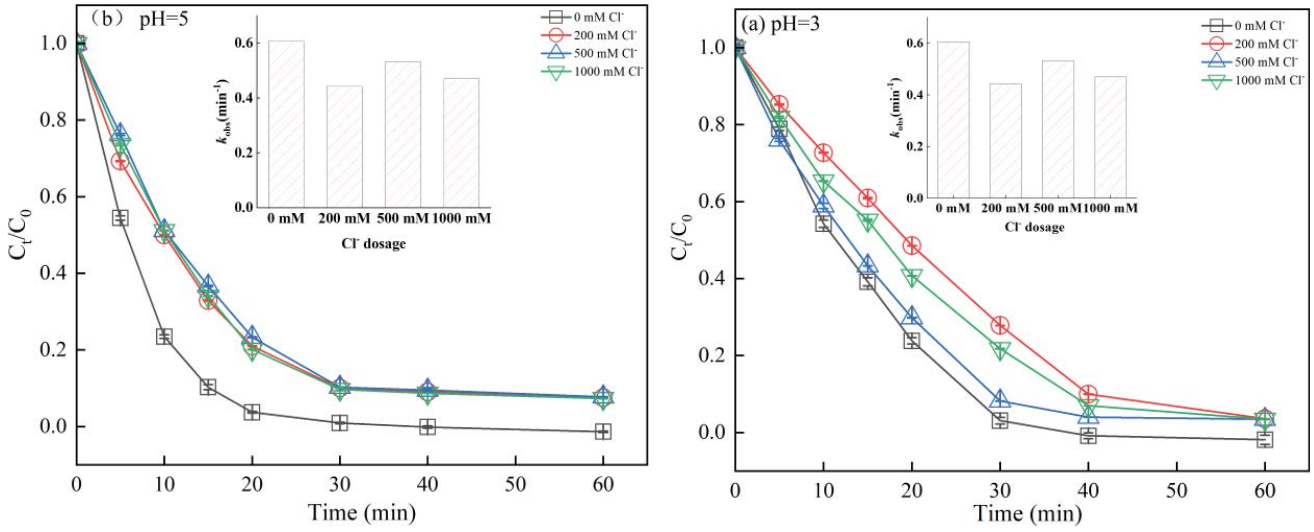

Fig. S2. (Continued)

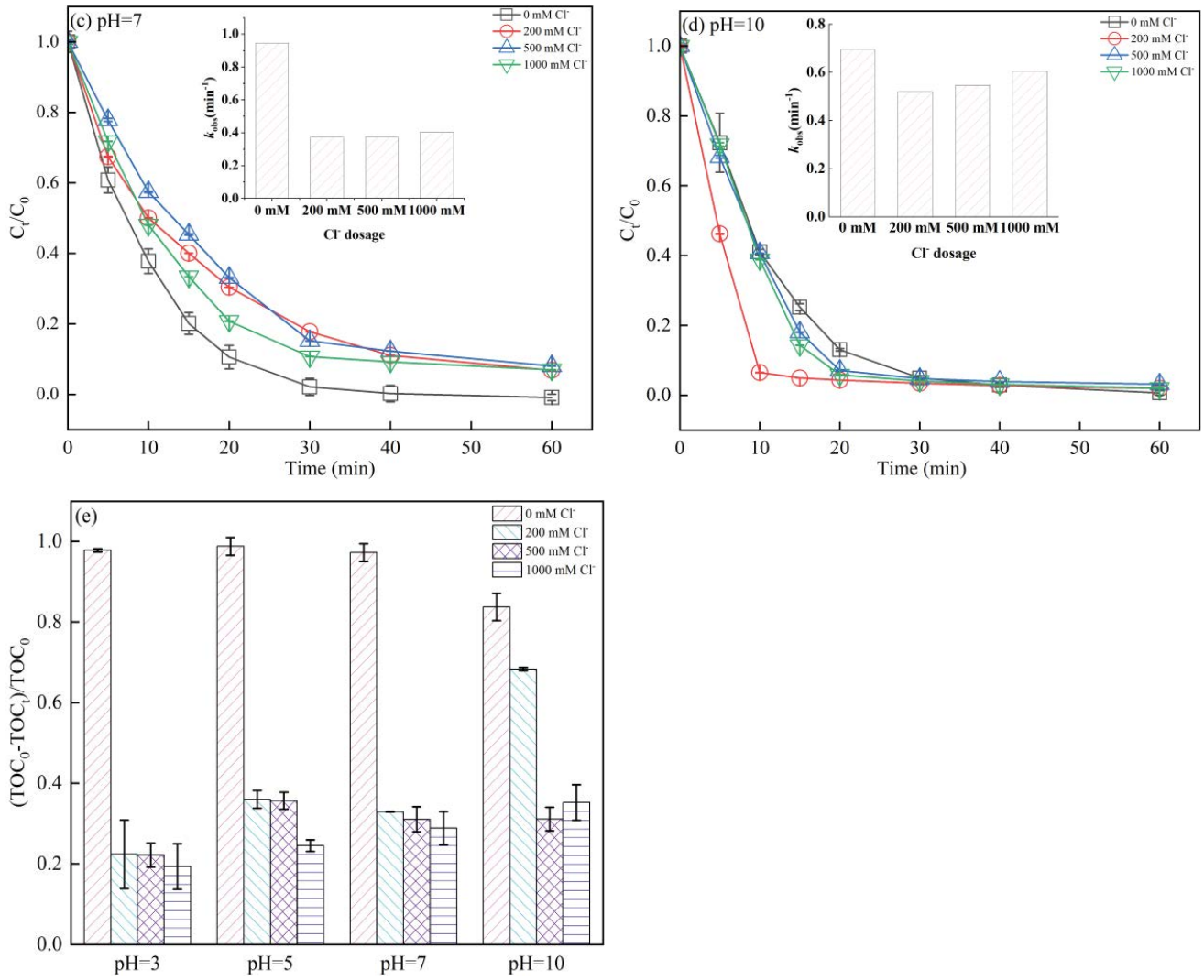

Fig. S2. Effects of various Cl^- contents on OrgII decolorization rate and pseudo-first-order rate constant at (a) pH 3, (b) pH 5, (c) pH 7, and (d) pH 10, and on (e) TOC removal rate. Experimental conditions: T = 25°C ± 1°C, $[OrgII]_0$ = 0.1 mM, $[PDS]_0$ = 10 mM.

S4. UV-VIS spectra of OrgII treated by UV/PDS in the presence of Cl–

The comparative analysis of Fig. S3a and b shows that there is no significant difference between the UV-VIS spectra of the control group without Cl^- and the experimental group with 1,000 mmol/L·Cl^-. With the extension of reaction time, there is no obvious new peak except for two characteristic peaks. Among them, 484 nm is the main characteristic absorption peak of OrgII, which corresponds to the azo bond of the chromogenic functional group, and 310 nm corresponds to the naphthalene ring structure of OrgII. The absorption peaks at 484 and 310 nm decreased gradually with the extension of reaction time, and the peak value was almost not captured after 60 min of reaction. Therefore, it was speculated that the azo double bond of OrgII was quickly disconnected with the reaction. The experiment showed that the dye wastewater of OrgII was rapidly decolorized. At the same time, according to the structural formula of OrgII, the structure of the naphthalene ring connected by the azo bond was also broken and opened. After 60 min of reaction, the control group (a) showed that the spectral line was almost flat, while the experimental group (b) showed that the spectral line fluctuated at 254 nm, which corresponded to aromatic compounds, possibly due to the oxidation of naphthalene ring by free radicals.

S5. GC-MS analysis

S5.1. GC-MS analysis of OrgII treated by UV/PDS process under pH 3

As shown in Fig. S4a, the gas chromatograph of 0 mM Cl^- showing the peaks corresponding to 3,5-dimethylbenzaldehyde, ethylbenzene, m-xylene, 1-(tert-butyl)-3-methylbenzene, and 2,2′-methylenebis(6-tert-butyl-4-methylphenol). As shown in Fig. S4b, the gas chromatograph of 100 mM Cl^- showing the peaks corresponding to ethylbenzene, o-xylene, p-phthalic acid, octadecanoic acid, hexadecanoic acid, azelaic acid, adipic acid, succinic acid, and 3-chloro-3-methylpentane.

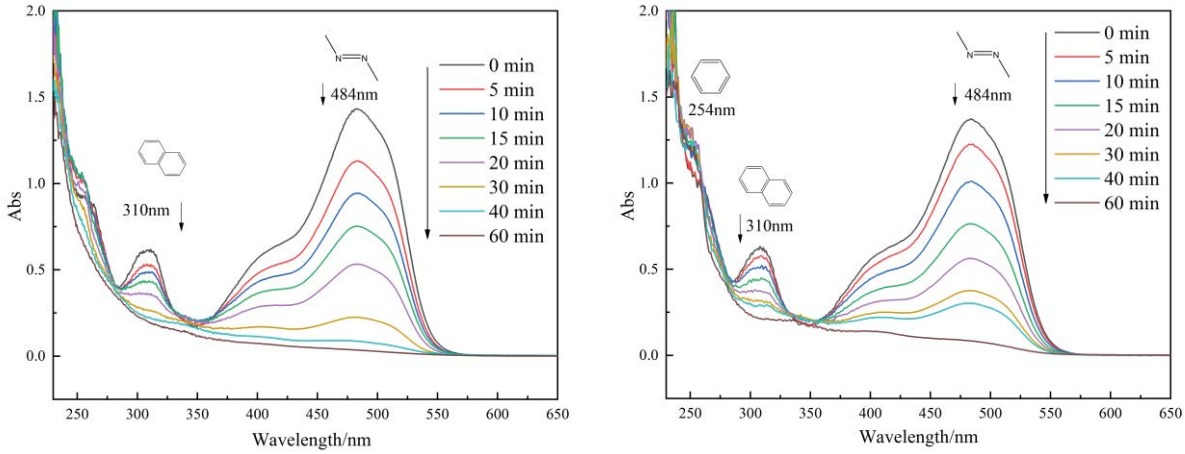

Fig. S3. UV-VIS spectra of OrgII treated by UV/PDS in the presence of Cl^-. (a) Cl^- free control group (b) 1,000 mM Cl^- experimental group, Experimental conditions: $[OrgII]_0$ = 0.1 mM, $[PDS]_0$ = 10 mM, pH = 3, and T = 25°C ± 1°C.

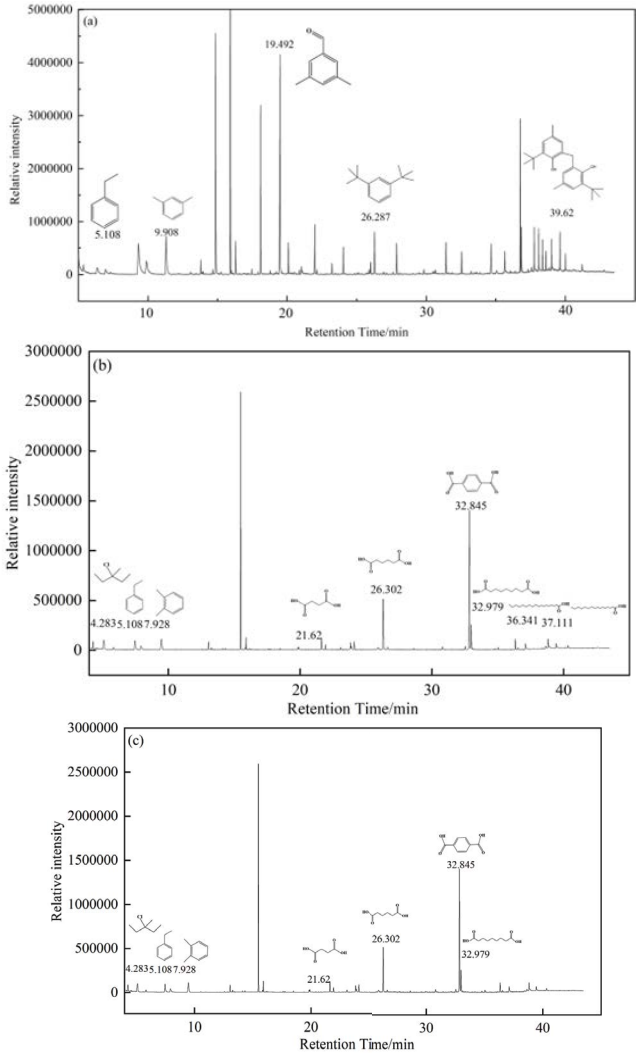

Fig. S4. GC-MS spectrum analysis of OrgII treated by UV/PDS process for (a) without Cl^-, (b) with Cl^- at 100 mM, and (c) with Cl^- at 100 mM and SO_4^{2-} at 100 mM. Experimental conditions: $[OrgII]_0$ = 0.1 mM, $[PDS]_0$ = 10 mM, pH = 3, and T = 25°C ± 1°C.

As shown in Fig. S4c, the gas chromatograph of 100 mM Cl^- and 100 mM SO_4^{2-} showing the peaks corresponding to ethylbenzene, o-xylene, p-phthalic acid, azelaic acid, adipic acid, succinic acid, and 3-chloro-3-methylpentane.

S5.2. GC-MS analysis of OrgII treated by UV/PDS process under pH 10

As shown in Fig. S5, the gas chromatograph of 100 mM Cl^- showing the peaks corresponding to ethylbenzene, o-xylene, p-phthalic acid, adipic acid, succinic acid, Pentane, and 3-chloro-3-methylpentane.

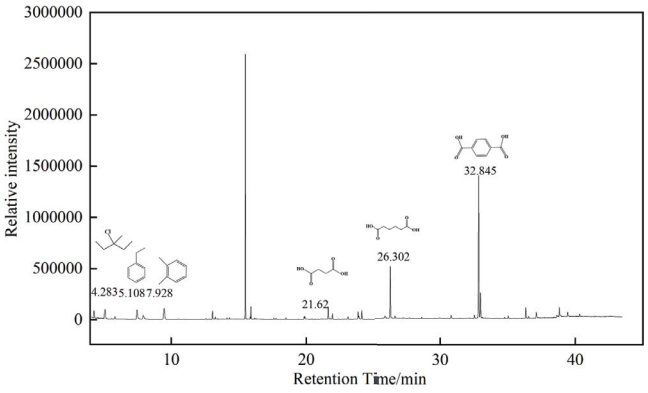

Fig. S5. GC-MS spectrum analysis of OrgII treated by UV/PDS process with Cl^- at 100 mM. Experimental conditions: $[OrgII]_0$ = 0.1 mM, $[PDS]_0$ = 10 mM, $[Cl^-]_0$ = 1,000 mM, pH = 10, and T = 25°C ± 1°C.